Depletion of SMC5/6 sensitizes male germ cells to DNA damage

G. Hwang[a], D. E. Ververb[b], M. A. Handel[c], G. Hamer[b], and P. W. Jordan[a,*]
[a]Department of Biochemistry and Molecular Biology, Bloomberg School of Public Health, Johns Hopkins University, Baltimore, MD 21205; [b]Reproductive Biology Laboratory, Center for Reproductive Medicine, Academic Medical Center, 1105 AZ Amsterdam, the Netherlands; [c]The Jackson Laboratory, Bar Harbor, ME 04609

ABSTRACT **The structural maintenance of chromosomes complex SMC5/6 is thought to be essential for DNA repair and chromosome segregation during mitosis and meiosis. To determine the requirements of the SMC5/6 complex during mouse spermatogenesis we combined a conditional knockout allele for *Smc5*, with four germ cell–specific Cre-recombinase transgenes, *Ddx4-Cre*, *Stra8-Cre*, *Spo11-Cre*, and *Hspa2-Cre*, to mutate *Smc5* in spermatogonia, in spermatocytes before meiotic entry, during early meiotic stages, and during midmeiotic stages, respectively. Conditional mutation of *Smc5* resulted in destabilization of the SMC5/6 complex. Despite this, we observed only mild defects in spermatogenesis. Mutation of *Smc5* mediated by *Ddx4-Cre* and *Stra8-Cre* resulted in partial loss of preleptotene spermatocytes; however, spermatogenesis progresses and mice are fertile. Mutation of *Smc5* via *Spo11-Cre* or *Hspa2-Cre* did not result in detectable defects of spermatogenesis. Upon exposure to gamma irradiation or etoposide treatment, each conditional *Smc5* mutant demonstrated an increase in the number of enlarged round spermatids with multiple acrosomes and supernumerary chromosome content. We propose that the SMC5/6 complex is not acutely required for premeiotic DNA replication and meiotic progression during mouse spermatogenesis; however, when germ cells are challenged by exogenous DNA damage, the SMC5/6 complex ensures genome integrity, and thus, fertility.**

Monitoring Editor
Orna Cohen-Fix
National Institutes of Health

Received: Jul 24, 2018
Revised: Sep 21, 2018
Accepted: Sep 27, 2018

INTRODUCTION

Structural maintenance of chromosome complexes (SMC) are conserved multiprotein complexes expressed in mitotic and meiotic cells and are involved in ensuring genome integrity. There are three classes of SMC complexes expressed in mammals: cohesin, condensing, and the SMC5/6 complex. Each SMC complex is comprised of two SMC proteins that interact with one another at their central hinge domains, and each protein folds back on itself via large coiled-coil domains emanating from the hinge (Murray and Carr, 2008). The juxtaposed N- and C-termini of each SMC protein form ATPase domains. The ATPase domains of the SMC5 and SMC6 heterodimers are bridged by a kleisin protein, NSMCE4, together with the E3 ubiquitin ligase NSMCE1 and the MAGE domain–containing protein NSMCE3 (Doyle *et al.*, 2010). Additionally, NSMCE2 is a SUMO E3 ligase component of the SMC5/6 complex, which interacts with the coiled-coil region of SMC5 (Andrews *et al.*, 2005; Zhao and Blobel, 2005; Potts and Yu, 2007).

The functions of cohesin and condensin during meiosis have been studied using various model organisms, including budding yeast, fission yeast, worms, and mouse. Cohesin is required to ensure repair of SPO11-induced double-strand breaks (DSBs), synaptonemal complex (SC) formation between homologues, sex body formation, and maintenance of sister chromatid cohesion (Klein *et al.*, 1999; Watanabe and Nurse, 1999; Pasierbek *et al.*, 2003; Bannister *et al.*, 2004; Revenkova *et al.*, 2004; Hodges *et al.*, 2005; Xu *et al.*, 2005; Baudrimont *et al.*, 2011; Herrán *et al.*, 2011; Caburet *et al.*, 2014; Hopkins *et al.*, 2014; Llano *et al.*, 2014; Severson and Meyer, 2014; Winters *et al.*, 2014; Phadnis *et al.*, 2015; Sakuno and Watanabe, 2015; Biswas *et al.*, 2016; Ward *et al.*, 2016). It has been

This article was published online ahead of print in MBoC in Press (http://www.molbiolcell.org/cgi/doi/10.1091/mbc.E18-07-0459) on October 3, 2018.

*Address correspondence to: P.W. Jordan (pjordan8@jhu.edu).

Abbreviations used: cKO, conditional knockout; SC, synaptonemal complex; SMC, structural maintenance of chromosomes.

demonstrated that condensin is required for DSB formation and repair, normal chromosome compaction, and biorientation of sister chromatids during meiosis (Mets and Meyer, 2009; Brito *et al.*, 2010; Lee *et al.*, 2011; Houlard *et al.*, 2015).

Researchers have used budding yeast, fission yeast, and worms to assess the requirements of the SMC5/6 complex during meiosis (Verver *et al.*, 2016a). The studies using yeast demonstrated that the SMC5/6 complex facilitates the resolution of joint molecules between homologous chromosomes before meiosis I (Wehrkamp-Richter *et al.*, 2012; Copsey *et al.*, 2013; Lilienthal *et al.*, 2013; Xaver *et al.*, 2013). Chromosome bridges were observed during meiosis in worm mutants of the SMC5/6 complex, which compromised chromosome segregation (Bickel *et al.*, 2010; Hong *et al.*, 2016). Localization of the SMC5/6 complex during mouse spermatogonial differentiation and meiosis has been reported (Gómez *et al.*, 2013; Verver *et al.*, 2013). Based on these studies, the SMC5/6 complex was implicated to have roles at the pericentromeric heterochromatin, the SC, and the sex body. However, using primary spermatogonia in culture, it was found that SMC5/6 subunit NSMCE2 is dispensable for spermatogonial differentiation (Zheng *et al.*, 2017).

To further assess the roles of the SMC5/6 complex during spermatogenesis, we created a *Smc5* conditional knockout (cKO) mouse model. We observed a decrease in preleptotene spermatocyte number when *Smc5* is mutated in spermatogonia, suggesting a role in premeiotic DNA replication. In contrast to studies in yeast and worm, we did not observe chromosome segregation defects during meiosis. However, using two different forms of exogenous DNA damage, ionizing radiation and etoposide, we determined that *Smc5* cKO germ cells exhibited increased instances of aberrant meiotic chromosome segregation after treatment. We propose that the SMC5/6 complex is essential only when meiotic DNA processing events are perturbed during mouse spermatogenesis.

RESULTS

Conditional mutation of Smc5 via germ cell–specific Cre-recombinase expression

As previously described, we produced mice with a cKO allele for *Smc5* (*Smc5 flox*), in which the fourth exon is flanked by Cre-recombinase target loxP sites (Figure 1A; see *Materials and Methods*; Hwang *et al.*, 2017). Cre-mediated deletion of the fourth exon results in a null allele of *Smc5* (*Smc5 del*). Mice with this allele were obtained only as heterozygotes, demonstrating that *Smc5* is essential for life. Mice heterozygous for the *Smc5 del* allele showed no visible morphological abnormalities during development and adult life. Therefore, we used *Smc5 flox/del* mice as controls and *Smc5 flox/del* mice that also harbored a germ cell–specific Cre transgene as our cKO animals (Figure 1B). As an additional control, we assessed mice with a single floxed *Smc5* allele (*Smc5 +/flox*) and the germ cell–specific Cre transgene. Four Cre-recombinase transgenes, *Ddx4-Cre*, *Stra8-Cre*, *Spo11-Cre*, and *Hspa2-Cre*, were used in this study. *Ddx4-Cre* expression is first detected in spermatogonia at embryonic day 15 (Gallardo *et al.*, 2007). *Stra8-Cre* is first expressed at 3 d postpartum, in spermatogonia through preleptotene stage spermatocytes (Sadate-Ngatchou *et al.*, 2008). *Spo11-Cre* is expressed as early as 10 d postpartum, which corresponds to early prophase, preleptotene/leptotene stage spermatocytes (Lyndaker *et al.*, 2013). *Hspa2-Cre* is expressed by 14 d postpartum, corresponding to midprophase, zygotene/pachytene-stage spermatocytes (Inselman *et al.*, 2010). Unlike the other three Cre-recombinase transgenes, the frequency of obtaining *Smc5 flox/del*, *Ddx4-Cre* cKO mice was lower than expected (4.84% obtained, 25% expected; Supplemental Figure 1A), suggesting that a proportion of these mice die during embryonic development.

We assessed the fertility, litter size, and Cre recombination efficiency of our cKO and control male mice by mating to wild-type C57BL6/J female mice (Supplemental Table S1). *Smc5* cKO mice using all four Cre-recombinase transgenes were fertile and produced litter sizes equivalent to control. Almost all pups obtained from the *Smc5* cKO males harbored the *Smc5 del* allele, indicating efficient Cre-mediated deletion of the fourth exon.

Conditional mutation of Smc5 results in destabilization of the SMC5/6 complex

We observed a pronounced decrease in SMC5 protein levels when assessing crude germ cell extracts from all four *Smc5* cKO mice via Western blot (Figure 1C and Supplemental Figures S1B and S2A). Moreover, the depletion of SMC5 protein was accompanied by a considerable decrease in protein levels for other SMC5/6 components. This demonstrates that SMC5 is essential for the stability of the SMC5/6 complex. Interestingly, we observed a decrease in SMC6 and NSMCE2 levels that was equivalent to the decrease detected for SMC5. The levels of the NSMCE1 and NSMCE4 proteins were reduced, but not to the same extent as the other SMC5/6 components. This difference could be attributed to their stabilization within the NSMCE1, 3, 4 trimer subcomplex, and there is evidence to suggest that these proteins have functions independent to the SMC5/6 complex (Palecek *et al.*, 2006; Hudson *et al.*, 2011; Kozakova *et al.*, 2015). Alternatively, this observation may be due to differences in individual protein turnover rates.

The most robust depletion of SMC5/6 components occurred with excision mediated by the *Stra8-Cre* transgene (Figure 1C and Supplemental Figure S2A). To further confirm this observation, we isolated early prophase (leptotene/zygotene stage), mid to late prophase (pachytene/diplotene stage) spermatocytes, and round spermatids using the STA-PUT density gradient germ cell purification method (La Salle *et al.*, 2009). The Cre recombination efficiency of the *Smc5 flox* allele was assessed via PCR (Figure 1D). Protein levels of each SMC5/6 component was substantially decreased in *Smc5 flox/del*, *Stra8-Cre* germ cells, complementing the results obtained from the whole germ cell extracts (Figure 1E and Supplemental Figure S2B).

Conditional mutation of Smc5 by Ddx4-Cre and Stra8-Cre results in depletion of preleptotene spermatocytes

The *Smc5 flox/del*, *Spo11-Cre* and *Smc5 flox/del*, *Hspa2-Cre* cKO mice did not show differences in testis weight compared with controls (Supplemental Figure S3, A, B, D, and E), and furthermore, tubule cross-sections from these mice showed no evidence of germ cell abnormalities (Supplemental Figure S3, C and F). In contrast, the *Smc5 flox/del*, *Ddx4-Cre* and *Smc5 flox/del*, *Stra8-Cre* cKO mice had a 20–25% reduction in testis weight compared with controls (Figure 2, A and B, and Supplemental Figure S1C). Tubule cross-sections of adult *Smc5 flox/del*, *Ddx4-Cre* and *Smc5 flox/del*, *Stra8-Cre* cKO mice showed that many tubules were deficient for one or more germ cell subtypes (Figure 2, C and D, and Supplemental Figure S1D). Close analysis of periodic acid–Schiff (PAS)-stained cross-sections revealed that the depletion of germ cells occurred at the preleptotene stage of spermatogenesis (Figure 2, E and F, and Supplemental Figure S1D). A- and B-type spermatogonia were not affected in these cKO mice. Moreover, there were clear signs of spermatogenesis recovery within the tubule sections, indicating the presence of functional spermatogonial stem cells and undifferentiated spermatogonia that were detected by LIN28 expression (Figure 2F).

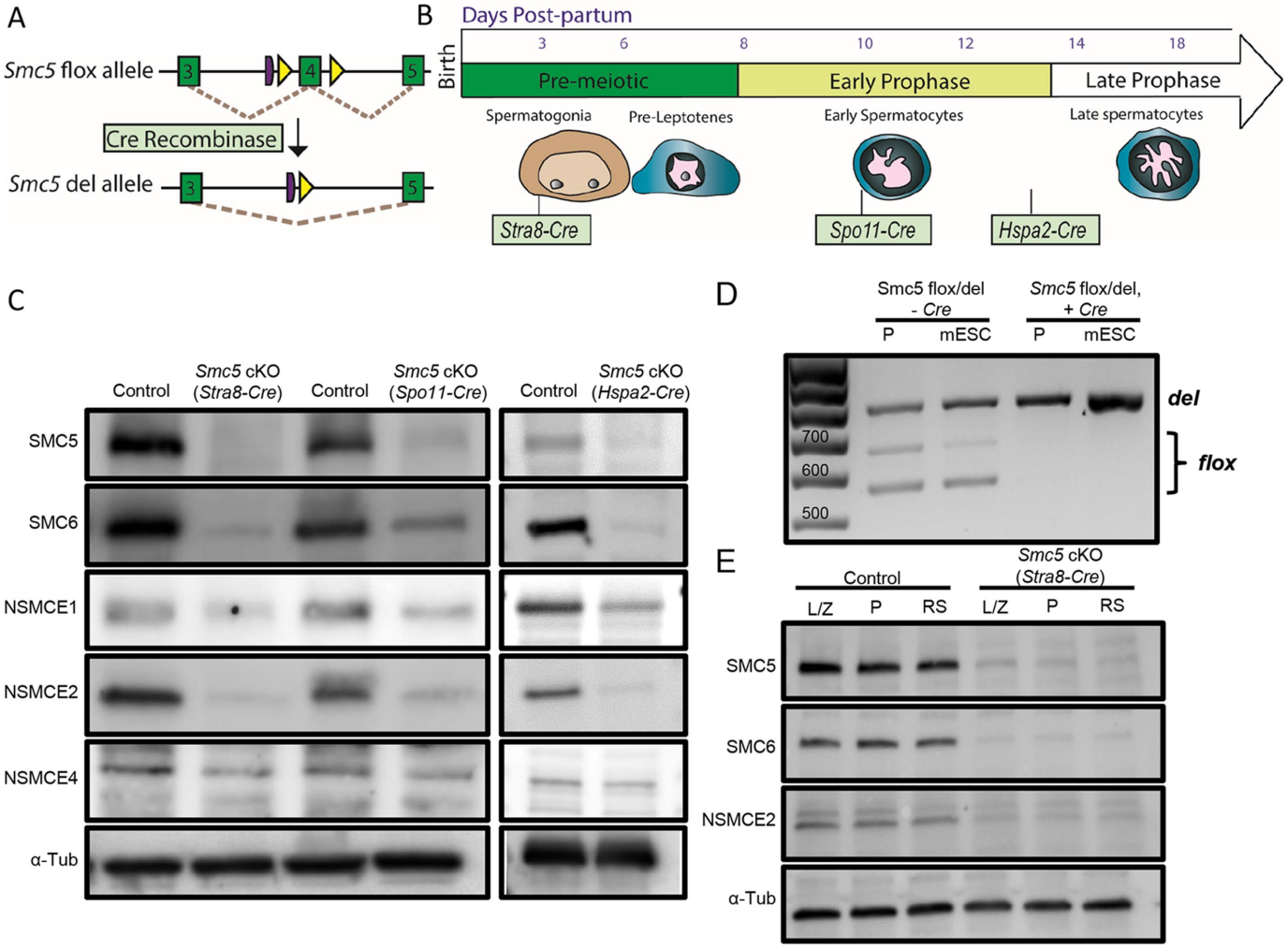

FIGURE 1: Conditional mutation of *Smc5* via germ cell–specific Cre-recombinase expression does not affect fertility but causes destabilization of the SMC5/6 complex. (A) Schematic of mouse *Smc5* floxed allele containing loxP sites (yellow triangle), flanking exon 4 (dark green box), and the resulting *Smc5* deletion allele after excision of exon 4 by Cre recombinase. The purple round-sided rectangle represents the remaining Frt site following FLP-mediated recombination of the original conditional ready tm1a allele (Hwang *et al.*, 2017). (B) Germ cell–specific Cre-recombinase expression timeline. Black lines indicate when the corresponding Cre is first expressed. *Ddx4-Cre* is not pictured; it is expressed in spermatogonia at embryonic day 15. (C) Protein extracts from crude germ cell isolates from control (*Smc5 flox/del*), and each *Smc5* cKO (*Smc5 flox/del, Germ cell–specific Cre*$^{tg/0}$); *Smc5* cKO (*Stra8-Cre*), *Smc5* cKO (*Spo11-Cre*), and *Smc5* cKO (*Hspa2-Cre*); were loaded on a 4–15% SDS–PAGE gradient gel and assessed for SMC5, SMC6, NSMCE1, NSMCE2, and NSMCE4 protein levels. α-Tubulin was used as the loading control. Extracts were all from mice ≥12 wk old. Protein levels of SMC5/6 components are reduced in all *Smc5* cKO extracts compared with controls. (D, E) Spermatocytes were purified via STA-PUT into specified prophase substages: leptotene/zygotene (L/Z; ~85% enrichment), pachytene (P; ~90% enrichment), and round spermatid (RS; ~95% enrichment). Spermatocytes were isolated from *Smc5 flox/del* (control) and *Smc5 flox/del, Stra8-Cre*$^{tg/0}$ (*Smc5* cKO) mice ≥12 wk old. (D) DNA agarose gel image of PCR products for genotyping, showing efficient deletion of the *Smc5* floxed exon 4 via Cre recombination. Lanes 1 and 2 represent *Smc5 flox/del,* without Cre recombinase: 763 base pairs del allele, 563 and 644 base pairs flox allele. Lanes 3 and 4 represent *Smc5 flox/del* with Cre recombinase: 763 base pairs del allele. Mouse embryonic stem cells were used as a control (mESC). (E) Protein extracts isolated from STA-PUT purified spermatocyte and round spermatids were loaded on a 4–15% SDS–PAGE gradient gel and assessed for SMC5, SMC6, and NSMCE2. α-Tubulin was used as the loading control. Protein levels of SMC5, SMC6, and NSMCE2 are reduced in all *Smc5* cKO extracts compared with controls. See Supplemental Figures S1 and S2 and Supplemental Table S1 for additional data.

To support our analysis, we assessed PCNA signal to determine the number of cells actively undergoing DNA replication per tubule (Figure 2G). We observed a significant decrease in the number of PCNA-positive cells per tubule in the *Smc5 flox/del*, *Stra8-Cre* cKO, supporting our initial observation that disappearance of germ cells occurred during the premeiotic S-phase (preleptotene; Figure 2H). In addition, TUNEL staining demonstrated an increase in apoptosis in the *Smc5 flox/del*, *Stra8-Cre* cKO mice (Figure 2I). We also assessed DAZL and SYCP3 chromosome axes signal to further distinguish spermatogonia and preleptotene spermatocytes from prophase I stages of spermatogenesis. The *Smc5 flox/del*, *Stra8-Cre* cKO displayed a decrease in the number of DAZL-positive, SYCP3-negative

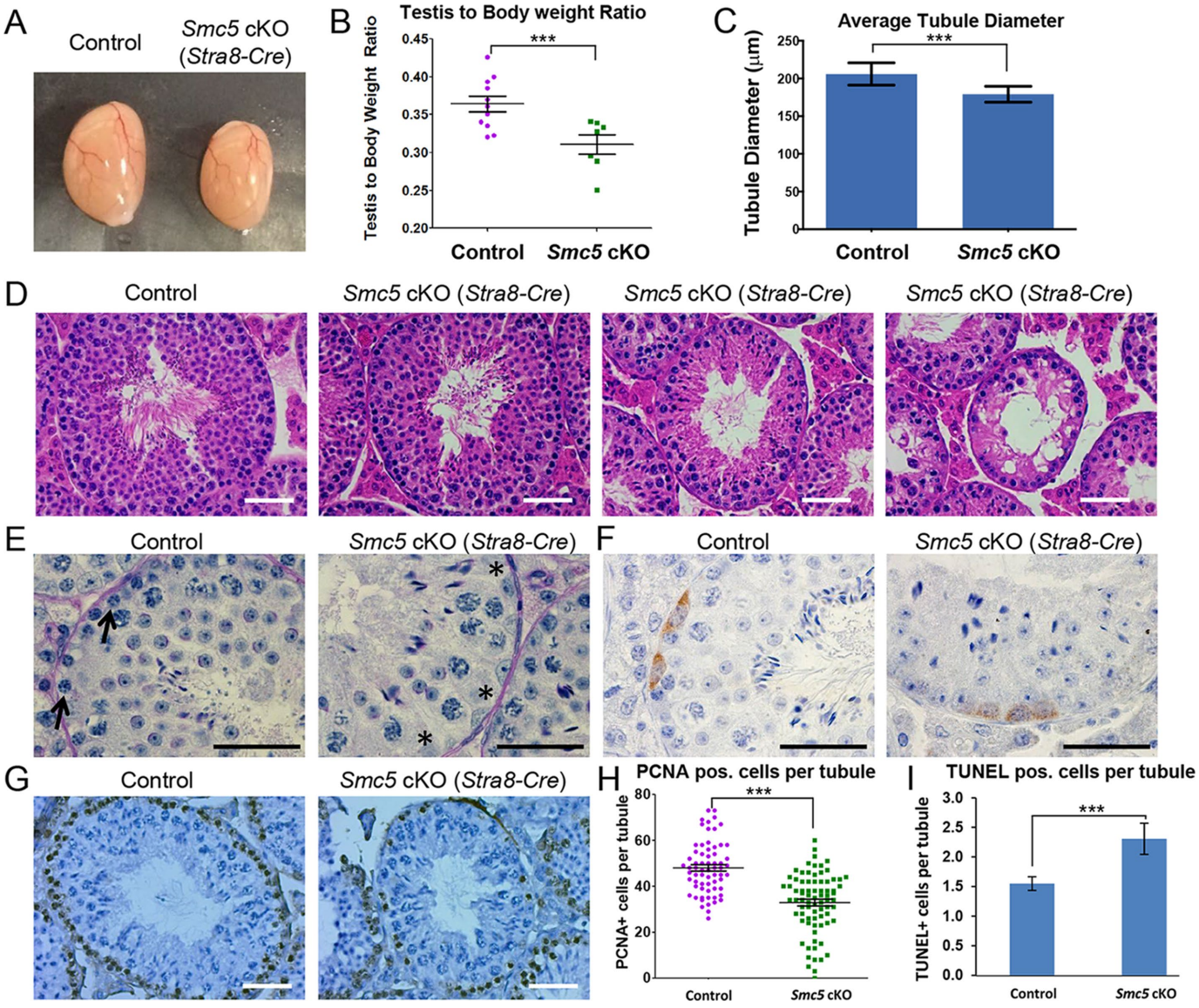

FIGURE 2: Conditional mutation of *Smc5* via Stra8-Cre results in depletion of preleptotene spermatocytes. (A–I) Phenotypic and histological assessments of testis from control and *Smc5* cKO (*Stra8-Cre*) mice ≥12 wk old. Note that *Smc5 flox/del, Stra8-cre*$^{tg/0}$ is written as *Smc5* cKO (*Stra8-Cre*). (A) Testis of adult control and *Smc5* cKO mice. (B) Assessment of adult testis to body weight ratio (mg/mg), whereby *Smc5* cKO (*Stra8-Cre*; $n = 7$, mean = 0.31) ratios are decreased compared with control ($n = 11$, mean = 0.36). Bars indicate mean and standard error. The *P* value (Mann-Whitney, two-tailed) for the indicated comparison is significant; $P < 0.0001$ (***). (C) Bar graph assessing average tubule diameter found in control (205.8 μm) and *Smc5* cKO (179.1 μm) testes with bars indicating standard error. The *P* value (Mann-Whitney, two-tailed) for the indicated comparison is significant; $P < 0.0001$ (***). (D) Tubule cross-sections of testes from adult control and *Smc5* cKO mice stained with hematoxylin and eosin. The three cross-sections displayed for *Smc5* cKO demonstrate the varied tubule morphology observed. Scale bar: 50 μm. (E) Periodic acid–Schiff staining of tubule cross-sections from control and *Smc5* cKO testes. Black arrows mark preleptotene spermatocytes that are missing in *Smc5* cKO mice (sites indicated by stars). Scale bar: 50 μm. (F) Periodic acid–Schiff staining of tubule cross-sections from control and *Smc5* cKO testes. Undifferentiated spermatogonia (brown) were detected using an antibody against LIN28. Scale bar: 50 μm. (G) Hematoxylin and eosin staining of tubule cross-sections from adult control and *Smc5* cKO mice testes. All actively replicating cells, including premeiotic cells, are marked with PCNA (brown). Scale bar: 50 μm. (H) Scatter dot–plot graph showing the reduction of PCNA-positive cells per tubule cross-section in adult *Smc5* cKO ($n = 78$, mean = 32.9) compared with control ($n = 66$, mean = 48) testes. Bars indicate mean and standard error. The *P* value (Mann-Whitney, two-tailed) for the indicated comparison is significant; $P < 0.0001$ (***). (I) Graph showing increased counts of TUNEL-positive (apoptotic) cells per tubule in adult *Smc5* cKO testes compared with control. The *P* value (Mann-Whitney, two-tailed) for the indicated comparison is significant; $P < 0.0001$ (***). See Supplemental Figures S1, S3, and S4 for additional data.

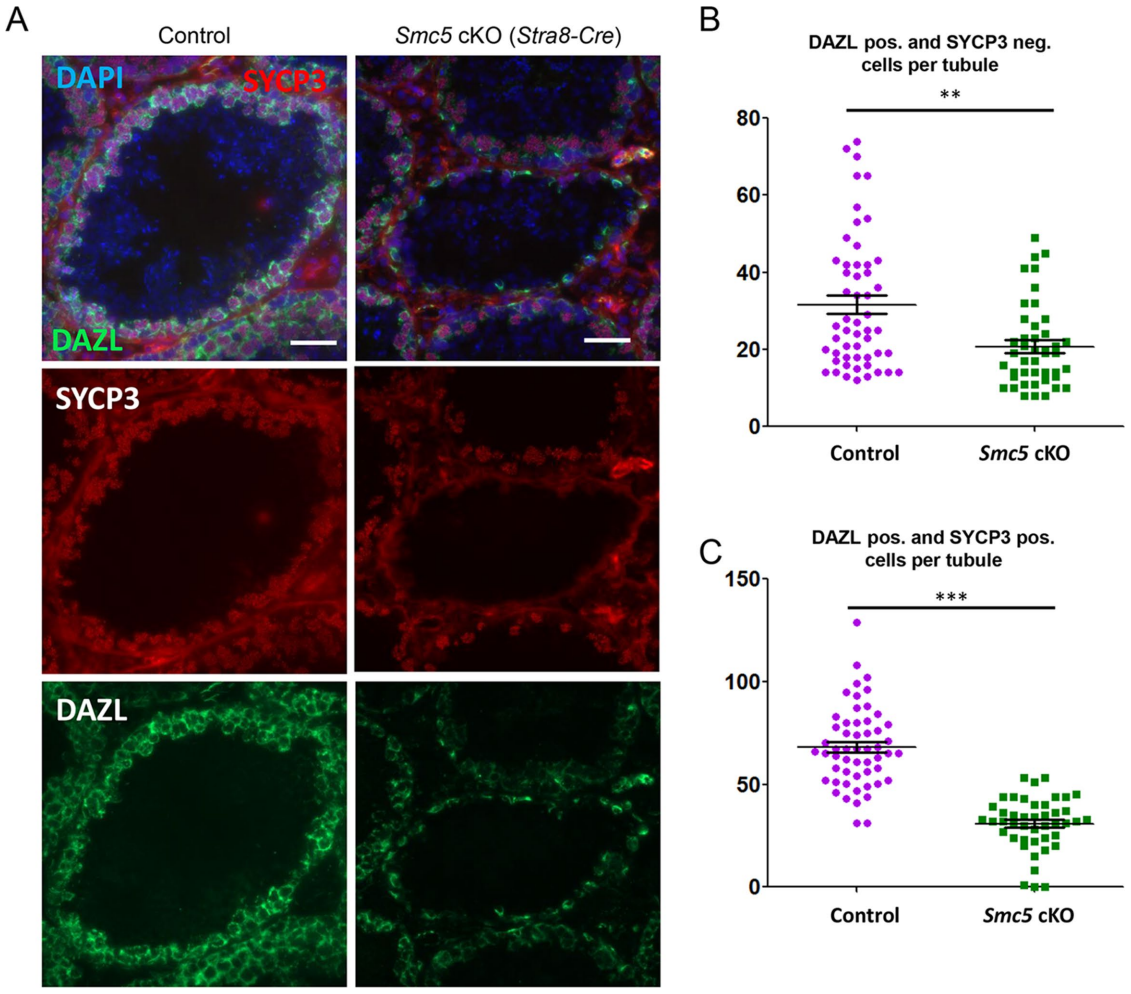

FIGURE 3: *Smc5 flox/del*, *Stra8-Cre*$^{tg/0}$ mutants display decrease in the number of pre-leptotene spermatocytes compared with the control. (A) Examples of tubule cross-sections of testes from adult control and *Smc5* cKO (*Stra8-Cre*) mice immunolabeled with antibodies against the SC lateral element protein SYCP3 (red) and DAZL (present in nucleus of spermatogonia and cytoplasm of meiotic cells, green) and counterstained with DAPI (DNA, blue). Scale bar: 50 μm. (B) Scatter dot–plot graph showing decreased number of DAZL-positive and SYCP3-negative cells per tubule in adult *Smc5* cKO ($n = 46$, mean = 20.50) compared with control ($n = 53$, mean = 31.62). Bars indicate mean and standard error. The *P* value (Mann-Whitney, two-tailed) for the indicated comparison is significant; $P < 0.0005$ (**). (C) Scatter dot–plot graph showing decreased number of DAZL-positive and SYCP3-positive cells per tubule in adult *Smc5* cKO ($n = 44$, mean = 30.84) compared with control ($n = 54$, mean = 68.15). Bars indicate mean and standard error. The *P* value (Mann-Whitney, two-tailed) for the indicated comparison is significant; $P < 0.0001$ (***).

cells and, consequently, this decrease appeared even greater in the DAZL and SYCP3-positive prophase I cells (Figure 3). To complement these data, we also assessed tubule cross-sections of juvenile mice undergoing the first wave of spermatogenesis. These analyses showed there was an increase in apoptosis (via TUNEL staining), and decreased number of PCNA-positive cells per tubule in *Smc5 flox/del*, *Stra8-Cre* cKO mice (Figure 4, A–D).

In yeast, it has been shown that absence of the SMC5/6 complex can lead to replication fork instability, inefficient replication restart, and formation of aberrant recombination intermediates (Murray and Carr, 2008). Therefore, we hypothesized that the subset of preleptotene stage spermatocytes undergoing apoptosis are affected by spontaneous errors during DNA replication. By assessing juvenile mice undergoing the first wave of spermatogenesis, we determined that depletion of SMC5/6 was correlated to increased RAD51 foci in premeiotic germ cells, suggesting that replication fork collapse and recombination intermediates occurred more predominantly in the *Smc5 flox/del*, *Stra8-Cre* cKO compared with controls (Figure 4, E and F).

Conditional mutation of Smc5 does not result in abnormal meiotic progression in mouse

Because meiotic recombination and chromosome segregation defects have been reported for SMC5/6 mutant yeast and worms (Bickel *et al.*, 2010; Wehrkamp-Richter *et al.*, 2012; Copsey *et al.*, 2013; Lilienthal *et al.*, 2013; Xaver *et al.*, 2013; Hong *et al.*, 2016), we assessed meiotic progression in our *Smc5* cKO mutants. The distribution of meiotic prophase stages analyzed was not different between the *Smc5 flox/del*, *Stra8-Cre* cKO and control (Figure 5, A and B). SC morphology and SC disassembly, together with sex body formation in the *Smc5 flox/del*, *Stra8-Cre* cKO were equivalent to the control (Figure 5, A and B, and Supplemental Figure S4). We did not observe any defects with respect to DNA repair as assessed by γH2AX staining (Figure 5A). We analyzed RAD51/DMC1 foci at early

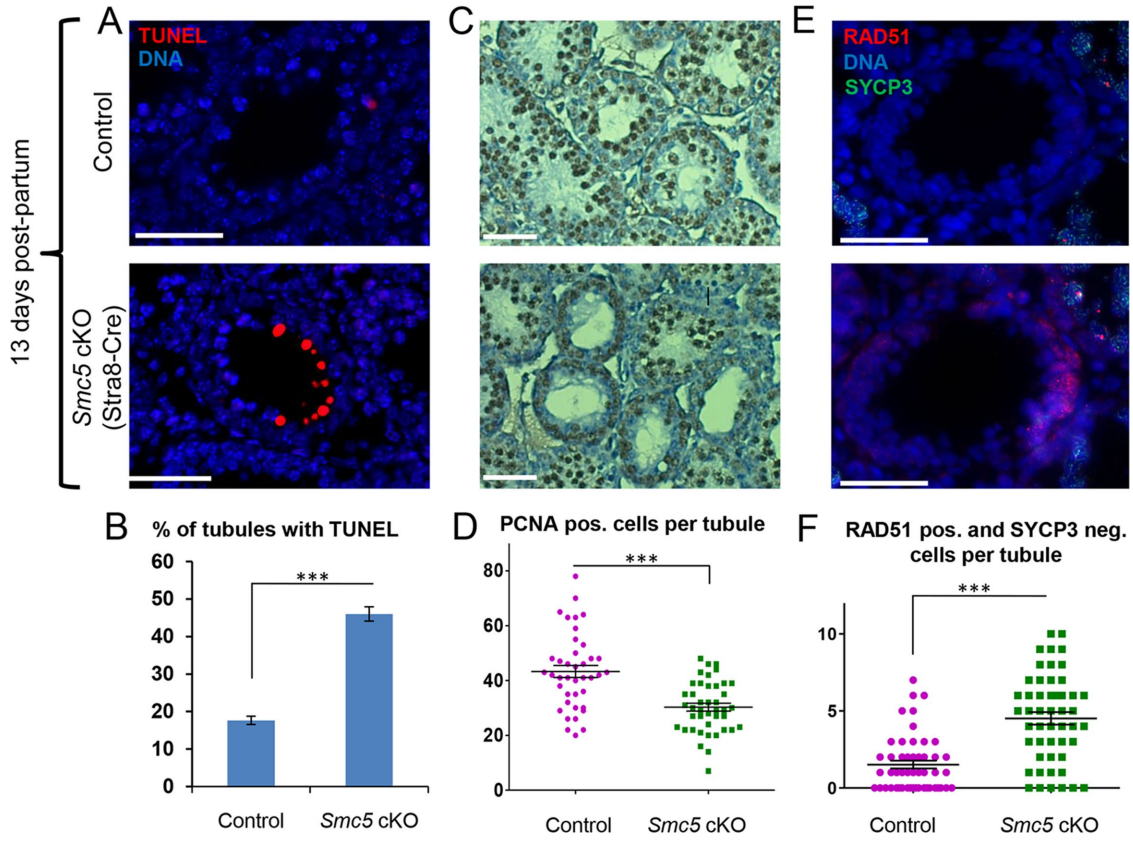

FIGURE 4: *Smc5* cKO juvenile mice, undergoing the first wave of spermatogenesis, show premeiotic cell defects. (A–C) Histological analysis of juvenile (13 d postpartum) control and *Smc5* cKO (*Stra8-Cre*) testes. (A) Tubule cross-sections stained with TUNEL and DAPI (red and blue, respectively). (B) Bar graph showing increased percentage of TUNEL-positive (apoptotic) tubules in juvenile *Smc5* cKO testes compared with control. (C) Tubule cross-sections stained with hematoxylin and eosin (blue) and PCNA (brown). (D) Scatter dot–plot graph showing decreased number of PCNA-positive cells per tubule in juvenile *Smc5* cKO ($n = 42$, mean = 30.2) compared with control ($n = 40$, mean = 43.3) testes. (E) Tubule cross-sections stained with RAD51, SYCP3, and DAPI (red, green, and blue, respectively). (F) Scatter dot–plot graph showing increased RAD51-positive, SYCP3-negative cells per tubule in juvenile *Smc5* cKO ($n = 50$, mean = 4.4) compared with control ($n = 50$, mean = 1.4) testes. Image scale bars: 50 µm. Graph bars indicate mean and standard error. The *P* values (Mann-Whitney, two-tailed) for the indicated comparisons are significant, $P < 0.0001$ (***).

pachytene stage and determined that the numbers were comparable between the control and cKO mice, including on the X-Y chromosome axes (Figure 5, C–F). Assessment of MLH1 foci indicated that there was no alteration in crossover frequency (Figures 5G and 4H). Additionally, there were no morphological differences in metaphase I chromosomes among *Smc5 flox/del*, *Stra8-Cre* cKO or control spermatocytes (Figure 5I). We also compared the meiotic prophase and metaphase stages in the *Smc5 flox/del*, *Ddx4-Cre*, *Smc5 flox/del*, *Spo11-Cre* and *Smc5 flox/del*, *Hspa2-Cre* cKO to littermate controls, and did not observe any differences (unpublished data).

Exposure of Smc5 cKO pachytene spermatocytes to exogenous DNA damage results in the formation of enlarged round spermatids with supernumerary chromosome number

Results of small interfering RNA (siRNA)-mediated knockdown and mutation studies using human cell lines reveal that depletion of the SMC5/6 complex leads to increased genome instability when exposed to exogenous DNA damage, including irradiation and etoposide exposures (Wu *et al.*, 2012; Payne *et al.*, 2014; Verver *et al.*, 2016b). Therefore, we assessed whether *Smc5* cKO prophase spermatocytes had elevated abnormalities when exposed to gamma irradiation and etoposide. Ionizing radiation induces a variety of DNA lesions, with DSBs being the most harmful (Dexheimer, 2013). Etoposide binds to the topoisomerase II-DNA complex, which induces the formation of DSBs (Heisig, 2009).

Adult *Smc5 flox/del*, *Ddx4-Cre*, *Smc5 flox/del*, *Stra8-Cre*, *Smc5 flox/del*, *Spo11-Cre* and *Smc5 flox/del*, *Hspa2-Cre* cKO and littermate controls were irradiated and assessed for defects at 5, 8, and 10 d postirradiation (Supplemental Figure S5). Five days postirradiation, germ cells that were in early pachytene stage (tubule stages I–III) at the time of irradiation will have progressed to late pachytene and diplotene stages, and late pachytene-stage germ cells (tubule stages X–XII) will have developed into to round spermatids (Ventelä *et al.*, 2012; Kent, 2014). At this time point, we did not observe a difference between mutant and control mice (Figure 6A). However, at 8 and 10 d postirradiation, when germ cells that were in early pachytene stage at the time of irradiation have become round spermatids, we observed a marked difference between the *Smc5* cKO mice and their littermate controls (Figure 6 and Supplemental Figure S6). Using PAS-stained tubule sections of *Smc5 flox/del*, *Ddx4-Cre* and *Smc5 flox/del*, *Stra8-Cre* cKO mice at 10 d postirradiation, we observed more than a 12- to 16-fold increase in the

number of enlarged round spermatids, commonly with two acrosome structures, a defect indicative of failure to segregate chromosomes during meiosis or cytokinesis failure (Figure 6, A–C, and Supplemental Figure S6). We also observed a two- to threefold increase in the number of enlarged spermatids in the *Smc5 flox/del*, *Spo11-Cre* and *Smc5 flox/del*, *Hspa2-Cre* compared with their littermate controls (Supplemental Figure S6). The reduced effect observed using *Spo11-Cre* and *Hspa2-Cre* is likely due to the timing of *Smc5* mutation, and, in the case of the *Spo11-Cre*, reduced excision efficiency (Supplemental Table S1).

Analysis of *Smc5 flox/del*, *Stra8-Cre* cKO tubule sections from 5, 8, and 10 d postirradiation (Figure 6A) revealed that spermatocytes irradiated at early or midpachynema (stages I–VII) developed into enlarged round spermatids, whereas those irradiated at late pachynema (stage VIII and beyond) formed normal sized spermatids. The *Smc5 flox/del*, *Stra8-Cre* cKO had a significant increase of spermatids with supernumerary chromosome number as assessed by centromere signals (Figure 6, D and E). To determine whether irradiation of the *Smc5 flox/del*, *Stra8-Cre* cKO results in failure to segregate chromosomes during meiosis or cytokinesis failure, we assessed irradiated juvenile mice that were undergoing the first wave of spermatogenesis. We observed cells from the *Smc5 flox/del*, *Stra8-Cre* cKO with lagging chromosomes, chromosome bridges, tri- or tetrapolar spindles, and abnormal chromosome condensation (Figure 7). This suggests that the enlarged spermatids observed in the *Smc5 flox/del*, *Stra8-Cre* cKO following irradiation are due to failure or aberrations in meiotic chromosome segregation.

Previous reports have shown that mutation of SMC5/6 components causes sensitivity to etoposide, and SMC5/6 colocalizes and interacts with topoisomerase IIα (Gómez *et al.*, 2013; Verver *et al.*, 2016b). To determine whether the *Smc5* mutant germ cells were also susceptible to etoposide, adult *Smc5 flox/del*, *Stra8-Cre* cKO and control mice were injected with etoposide and assessed for defects 3, 5, and 8 d postinjection (Figure 8). Etoposide exposure caused a similar phenotype as irradiation. At 3 and 5 d postinjection, we did not observe a difference between mutant and control mice (Figure 8A). Following 8 d of etoposide exposure, an increase in the number of enlarged spermatids, often with two acrosomes, was observed in the *Smc5 flox/del*, *Stra8-Cre* cKO (Figure 8B).

DISCUSSION

SMC5/6 plays a role during premeiotic DNA replication

Analysis of testes of the *Smc5 flox/del*, *Ddx4-Cre* and *Smc5 flox/del*, *Stra8-Cre* cKOs reveals germ cell loss at the preleptotene stage. These cells are undergoing premeiotic DNA replication, and we propose that the SMC5/6 complex is required to efficiently ensure genomic integrity during this process. Depletion of the SMC5/6 complex has been shown to hinder DNA replication progression in human RPE-1 cells. Upon siRNA-mediated knockdown of Smc5 or Smc6, DNA replication in RPE-1 cells progresses at a much slower rate, with a concomitant generation of replication-related DNA damage (Gallego-Paez *et al.*, 2014). As only a subset of preleptotene stage spermatocytes are affected in the *Smc5 flox/del*, *Ddx4-Cre* cKO and *Smc5 flox/del*, *Stra8-Cre* cKO, we predict that the SMC5/6 complex is particularly important when DNA replication processes are hindered in some way, such as a replication fork collapse. The observed increase in RAD51 signal in premeiotic germ cells in the *Smc5 flox/del*, *Stra8-Cre* cKO supports this hypothesis. Furthermore, research has shown that Smc5/6 mutant yeast and human cell lines are sensitive to DNA replication perturbations, such as hydroxyurea exposure (Ampatzidou *et al.*, 2006; Branzei *et al.*, 2006; Bermúdez-López *et al.*, 2010; Payne *et al.*, 2014).

Smc5 expression is not required for meiosis during mammalian spermatogenesis

Previous studies using yeast and worms implicate the SMC5/6 complex as important for mediating meiotic recombination events (Bickel *et al.*, 2010; Wehrkamp-Richter *et al.*, 2012; Copsey *et al.*, 2013; Lilienthal *et al.*, 2013; Xaver *et al.*, 2013; Hong *et al.*, 2016). Therefore, it was unexpected to find no evidence that the SMC5/6 complex is required for mouse spermatogenesis and male fertility. Although one concern could be that mutation of the floxed *Smc5* allele was not efficient, genotyping data indicated that *Ddx4-Cre*, *Stra8-Cre*, and *Hspa2-Cre* were close to 100% efficient in excision. The *Spo11-Cre* was less efficient, but even so, a mosaic meiotic phenotype would be expected. Furthermore, analysis of purified primary spermatocytes and round spermatids from *Smc5*, *Stra8-Cre* cKO mice confirmed the efficiency of *Smc5* excision via PCR, as well as depletion of the SMC5 protein and other SMC5/6 components. Despite the efficiency of the *Stra8-Cre*, we did not observe defects in meiotic prophase I events that include DNA damage repair, SC formation, crossover levels, sex body formation, and chiasmata morphology. Therefore, we can conclude that *Smc5* expression during spermatogenesis is not essential for meiotic progress and fertility in male mice.

SMC5/6 is important for maintaining genome integrity of pachytene-stage spermatocytes following exogenous DNA damage

As we did not observe a defect in the progression of meiosis in our *Smc5* cKO models, we hypothesized that the SMC5/6 complex is not required for meiosis during spermatogenesis, except when DNA processing events are perturbed. To test this hypothesis, we used gamma irradiation and etoposide to sensitize cells with DNA damage. Interestingly, spermatocytes staged at early and midpachynema at the time of treatment were affected by irradiation and etoposide exposure, causing the formation of enlarged round spermatids, which had two acrosomes and supernumerary chromosome content. In contrast, the late pachytene-stage spermatocytes were not affected in this way by irradiation, and formed normal sized spermatids. This distinction between the earlier and later stages of pachynema could be explained by differing DNA template preference during DNA repair. At early to midpachytene stage, there is a mechanism that biases toward interhomologue recombination over intersister recombination (Wojtasz *et al.*, 2009; Lao and Hunter, 2010). However, this bias is lost during late pachynema, thus facilitating repair of DSBs via intersister recombination (Moens *et al.*, 1997; Kauppi *et al.*, 2011). Endogenous DNA damage induced during the earlier stages of pachytene could result in the formation of complex joint molecules, involving homologues and sister chromatids, which, in absence of the SMC5/6 complex, may not be resolved before meiotic divisions. This hypothesis is supported by the chromosome segregation failure observed in the *Smc5* cKO following irradiation. In the case of the late pachytene stage, repair of the endogenous DNA damage might be facilitated primarily by intersister repair, as interhomologue recombination bias is relaxed, and these intermediates may be more easily resolved before chromosome segregation. An alternative explanation is that spermatocytes that are exposed to exogenous DNA damage during early and midpachynema are normally subject to pachytene checkpoint–mediated arrest and apoptotic death; however, in the absence of SMC5/6 these spermatocytes escape the checkpoint and form abnormal spermatids. This would suggest that SMC5/6 is a component of DNA damage checkpoint responses, or that the DNA intermediates that accumulate in the absence of SMC5/6 are not

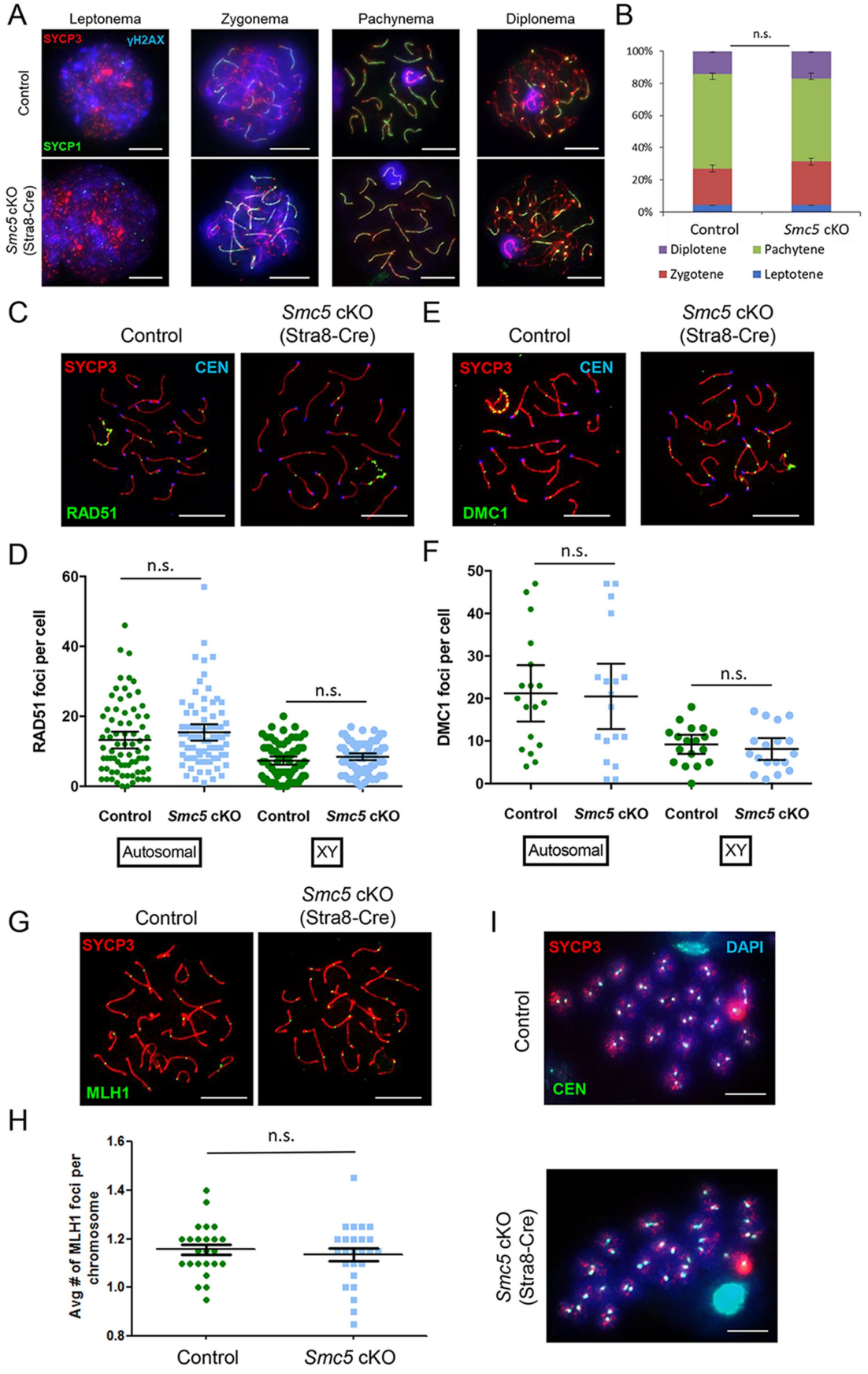

FIGURE 5: Conditional mutation of *Smc5* does not result in abnormal meiotic prophase progression in male mice. (A–I) No differences were observed when comgparin chromatin spread preparations from juvenile control and *Smc5* cKO (*Stra8-Cre*) germ cells staged at prophase to metaphase I. Assessments were using germ cells from mice ≥8 wk

recognized by the pachytene checkpoint. The latter is supported by studies in fission yeast, which have demonstrated that recombination DNA intermediates in an *smc6* mutant background are not recognized by the G2/M checkpoint (Ampatzidou *et al.*, 2006).

In budding yeast, the Smc5/6 complex was demonstrated to be required to inhibit the formation of complex joint molecules, which involve recombination intermediates between sisters and homologues (Copsey *et al.*, 2013; Xaver *et al.*, 2013). Furthermore, the budding yeast Smc5/6 complex is required for appropriate loading of the Mus81-Mms4/Eme1 resolvase complex to chromatin, and subsequent resolution of intersister and multiple chromatid joint molecules, which appears to be a conserved function in fission yeast (Wehrkamp-Richter *et al.*, 2012; Copsey *et al.*, 2013; Xaver *et al.*, 2013). In the mouse, the MUS81-EME1 complex is required for the resolution of ~5–10% of crossovers, which cannot be processed as noncrossovers by the BLM helicase (Holloway *et al.*, 2008, 2011). We attempted to determine whether the localization of the MUS81-EME1 complex in our spermatocytes was affected; however, immunostaining was not successful.

Conclusion

We have determined that the depletion of the SMC5/6 complex does not lead to meiotic failure during mouse spermatogenesis. However, we do observe a partial loss of premeiotic germ cells, suggesting a role in efficient premeiotic DNA replication. We also demonstrate that the SMC5/6 complex is important for a proficient response to exogenous DNA damage in prophase spermatocytes. We propose that the SMC5/6 complex acts as a DNA damage response surveillance complex. When genomic integrity is compromised, the SMC5/6 complex ensures that DNA repair processes are controlled to avoid complex recombination intermediates that would otherwise result in germ cell apoptosis or cause errors during chromosome segregation.

MATERIALS AND METHODS

Animal use and care

Mice were bred by the investigators at The Jackson Laboratory (JAX, Bar Harbor, ME) and Johns Hopkins University (JHU, Baltimore, MD) in accordance with criteria of the National Institutes of Health (NIH) and the U.S. Department of Agriculture. All animal procedures were conducted with approval from the Institutional Animal Care and Use Committees (IACUC) of The Jackson Laboratory and JHU.

Mice and husbandry

Creation of mice with the *Smc5 flox* and *Smc5 del* alleles was previously described (Hwang *et al.*, 2017). Heterozygous *Smc5 del* mice were bred to mice with germ cell–specific Cre-recombinase transgenes; *Ddx4-Cre* (B6.FVB-Tg[Ddx4-cre]1Dcas/KnwJ, Stock no. 018980; JAX), *Stra8-Cre* (B6.FVB-Tg[Stra8-icre]1Reb/LguJ, Stock no. 017490; JAX), *Spo11-Cre* (Lyndaker *et al.*, 2013), and *Hspa2-Cre* (C57BL/6-Tg[Hspa2-cre]1Eddy/J, Stock no. 008870; JAX), which resulted in progeny heterozygous for the *Smc5 del* allele and hemizygous for the germ cell–specific transgenes. These mice were bred to homozygous *Smc5 flox* mice to derive cKO (*Smc5 flox/del, germ cell–specific Cre*) and controls (*Smc5 flox/del* and *Smc5 +/flox, germ cell–specific Cre*) genotypes.

For fertility testing, 8- to 12-wk-old cKO and control males were singly housed with wild-type C57BL6/J females. Pregnant females were monitored daily, and viable pups were counted on the first day of life. Subsequently, genotyping samples were taken from each pup to determine the efficiency of Cre-mediated excision of the floxed fourth exon of the *Smc5* allele.

Induction of DNA damage via irradiation

Adult mice were irradiated with a single sublethal dose (5 Gy) using a 137Cs source (Hamer *et al.*, 2003). The mice were monitored daily before being killed 5, 8, and 10 d following irradiation.

Juvenile mice at 16 d postpartum were irradiated with a single sublethal dose (1.3 Gy) using a 137Cs source (Forand *et al.*, 2004). After irradiation, the mice were monitored daily before being killed at 23 d postpartum. Testes were extracted for spermatocyte squash preparation.

Induction of DNA damage via etoposide

For etoposide assessment, adult mice were injected intraperitoneally with a single dose of etoposide (80 mg/kg body weight; Sigma; Lee *et al.*, 1995; Marchetti *et al.*, 2006). After injection, the mice were monitored daily before being killed at 3, 5, or 8 d after treatment.

old. (A) Chromatin spreads were immunolabeled with antibodies against γH2AX (blue), the SC lateral element protein SYCP3 (red), and the SC central element protein SYCP1 (green). Scale bar: 10 µm. (B) Bar graph showing comparable distributions of prophase stages in control and *Smc5* cKO testes. Black bars indicate standard error. The *P* values (Mann-Whitney, two-tailed) for the indicated comparisons are not significant (n.s.). (C, E) Chromatin spread preparations were immunolabeled with antibodies for the SC lateral element protein SYCP3 (red), CEN (kinetochore/centromere marker) and DNA repair proteins RAD51 or DMC1 (green). (D) Scatter dot–plot graph showing RAD51 foci counts per cell on the autosomal chromosomes or the XY chromosome of juvenile control mice ($n = 74$, autosomal average = 13.22, XY mean = 7.34) and *Smc5* cKO mice ($n = 75$, autosomal mean = 15.40, XY average = 8.44). Bars indicate mean RAD51 foci number per cell with 95% confidence interval. The *P* values (Mann-Whitney, two-tailed test) for the indicated comparisons are not significant (n.s.). (F) Scatter dot–plot graph showing DMC1 foci counts per cell on the autosomal chromosomes or the XY chromosome of juvenile control mice ($n = 18$, autosomal mean = 21.22, XY mean = 9.22) and *Smc5* cKO mice ($n = 18$, autosomal mean = 20.50, XY mean = 8.11). Bars indicate mean DMC1 foci number per cell with 95% confidence interval. The *P* values (Mann-Whitney, two-tailed) for the indicated comparisons are not significant (n.s.). (G) Chromatin spreads were immunolabeled with antibodies, the SC lateral element protein SYCP3 (red), and the MLH1 (crossover protein, green). (H) Scatter dot–plot graph showing no significant difference in the mean number of MLH1 foci per chromosome axis when comparing control ($n = 24$, mean = 1.16) and *Smc5* cKO ($n = 25$, mean = 1.14) chromosome spread preparations. Bars indicate the average with standard error. The *P* value (Mann-Whitney, two-tailed test) for the indicated comparison is not significant (n.s.). (I) No differences were observed in chromatin spread preparations of control and *Smc5* cKO (*Stra8-Cre*) germ cells at metaphase I after treatment with okadaic acid. Chromatin spreads were immunolabeled with antibodies against the SC lateral element protein SYCP3 (red) and CEN (kinetochore/centromere marker, blue) and counterstained with DAPI (DNA, blue). Scale bar: 10 µm. See Supplemental Figure S5 for additional data.

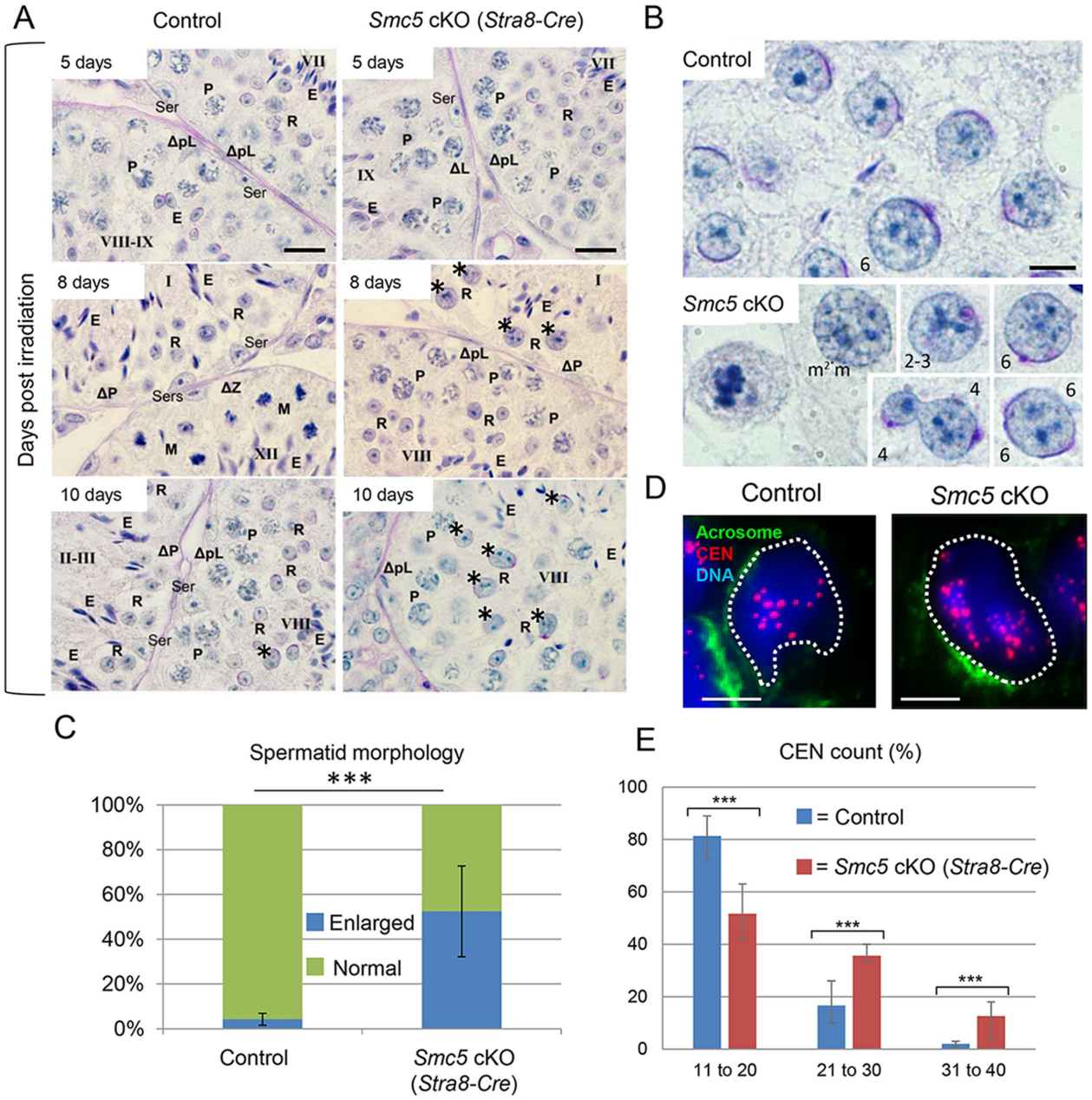

FIGURE 6: Conditional mutation of *Smc5* results in increased sensitivity to gamma irradiation, producing enlarged round spermatids with supernumerary centromeres after irradiation. Adult mice (8–12 wk of age) were exposed to gamma irradiation and assessed. (A) Tubule cross-sections of adult control and *Smc5* cKO (*Stra8-Cre*) mice testes with periodic acid–Schiff staining extracted at 5, 8, or 10 d postirradiation with 5 Gy. Markers: (*) abnormal enlarged round spermatids, (Ser) Sertoli cell, (pL) preleptotene stage, (L) leptotene stage, (Z) zygotene stage, (P) pachytene stage, (M) metaphase stage, (R) round spermatid, and (E) elongated spermatid. Roman numerals correspond to the seminiferous tubule stage. The Δ symbol indicates absence of marked cell type. *Smc5* cKO cross-sections display increased numbers of abnormal enlarged spermatids compared with the controls at 8 and 10 d postirradiation. Scale bar: 20 μm. (B) Magnified images of tubule cross-sections for control and *Smc5* cKO testes with periodic acid–Schiff staining, showing examples of normal and abnormal round spermatids. Round spermatids in *Smc5* cKO testes display an array of abnormalities, such as increase in size, atypical cell shape, and multiple acrosomes. Acrosomes on round spermatids are stained in purple. Numbers indicate stage of round spermatid development. Scale bar: 5 μm. (C) Bar graph showing significantly increased percentage of spermatids with enlarged morphology in *Smc5* cKO testes ($n = 513$) compared with the control ($n = 2291$) 10 d postirradiation. Bars indicate the average with SD. The *P* value (Mann-Whitney, two-tailed) for the indicated comparison is significant; $P < 0.0001$ (***). (D) Example of round spermatids from control and *Smc5* cKO observed 10 d postirradiation. Spermatids were immunolabeled with an antibody for CEN (kinetochore/centromere marker, red) and stained with lectin PNA-AF488 conjugate to mark the acrosome (green) and DAPI to detect the DNA (blue). Scale bar: 5 μm. (E) Graph showing counts of CEN (kinetochore/centromere marker) in control and *Smc5* cKO testes 10 d postirradiation. The *P* values (Mann-Whitney, two-tailed) for the indicated comparisons are significant, $P < 0.0001$ (***). See Supplemental Figures S6 and S7 for additional data.

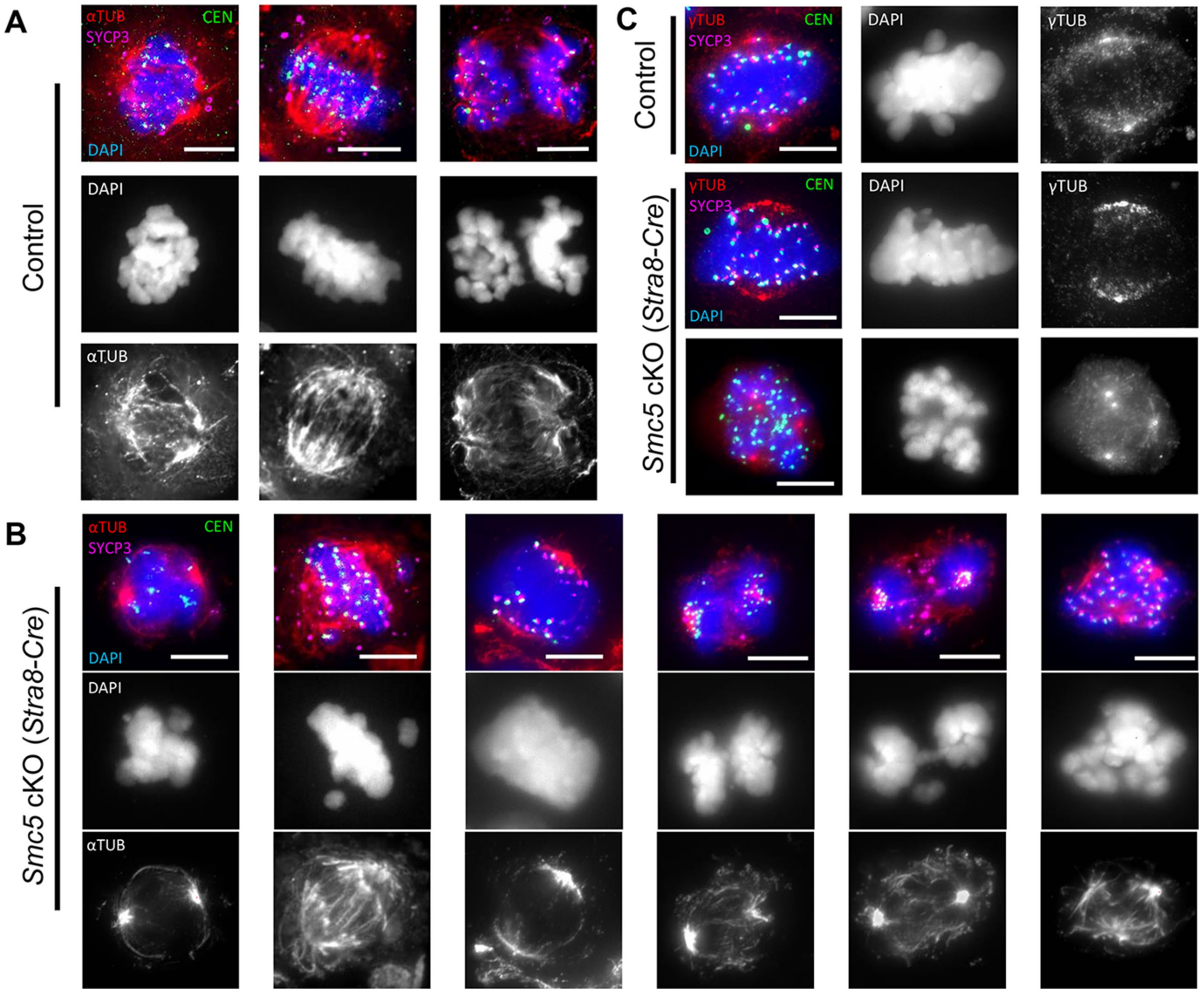

FIGURE 7: Conditional mutation of *Smc5* results in abnormal spindle formation and chromosome segregation errors after irradiation. (A–C) Immunostaining on tubule squash preparations of primary spermatocytes from control and *Smc5* cKO (*Stra8-Cre*) mice undergoing meiotic chromosome segregation following irradiation. Mice were 16 d old at the time of irradiation, and 23 d old at the time of analysis. Scale bar: 10 μm. (A, B) Triple-immunolabeling of primary spermatocytes with antibodies against CEN (green, kinetochore/centromere marker), the SC lateral element protein SYCP3 (pink), and α-tubulin (red, α-TUB) and counterstaining of chromatin with DAPI (blue) of germ cells. (A) Representative meiotic cells from control mice at metaphase I or undergoing anaphase I. (B) Representative meiotic cells from *Smc5* cKO mice at metaphase I or undergoing anaphase I. *Smc5* cKO spermatocytes show a range of chromosome condensation and segregation errors, including lagging chromosomes, tripolar spindles, and chromosome bridging. (C) Triple-immunolabeling of primary spermatocytes with antibodies against CEN (green, kinetochore/centromere marker), the SC lateral element protein SYCP3 (pink), and γ-tubulin (red, γ-TUB) and counterstaining of chromatin with DAPI (blue) of germ cells from control and *Smc5* cKO mice. A majority of *Smc5* cKO spermatocytes show normal bipolar spindles; however, there are incidences of four spindle poles (bottom panel), indicative of chromosome segregation failure.

Histological analysis and TdT-mediated dUTP nick end labeling (TUNEL) assay

Testes were either fixed in Bouins fixative or cryopreserved using Tissue-Tek optimal cutting temperature compound (O.C.T.; Sakura Finetek). Fixed tissues were embedded in paraffin and serial sections of 5-μm thickness were placed onto slides and stained with hematoxylin and eosin or PAS. For the TUNEL assay, sections were deparaffinized and apoptotic cells were detected using the in situ BrdU-Red DNA fragmentation (TUNEL) assay kit (Abcam) and counterstained with 4′,6-diamidino-2-phenylindole (DAPI). Cryopreserved testes were sectioned at a 5-μm thickness in series using a Cryostat (Thermo Scientific CyroStar NX70). Cryopreserved testes were subsequently fixed (1% paraformaldehyde [PFA], 0.1% Triton X in 1× phosphate-buffered saline [PBS]), and subjected to standard

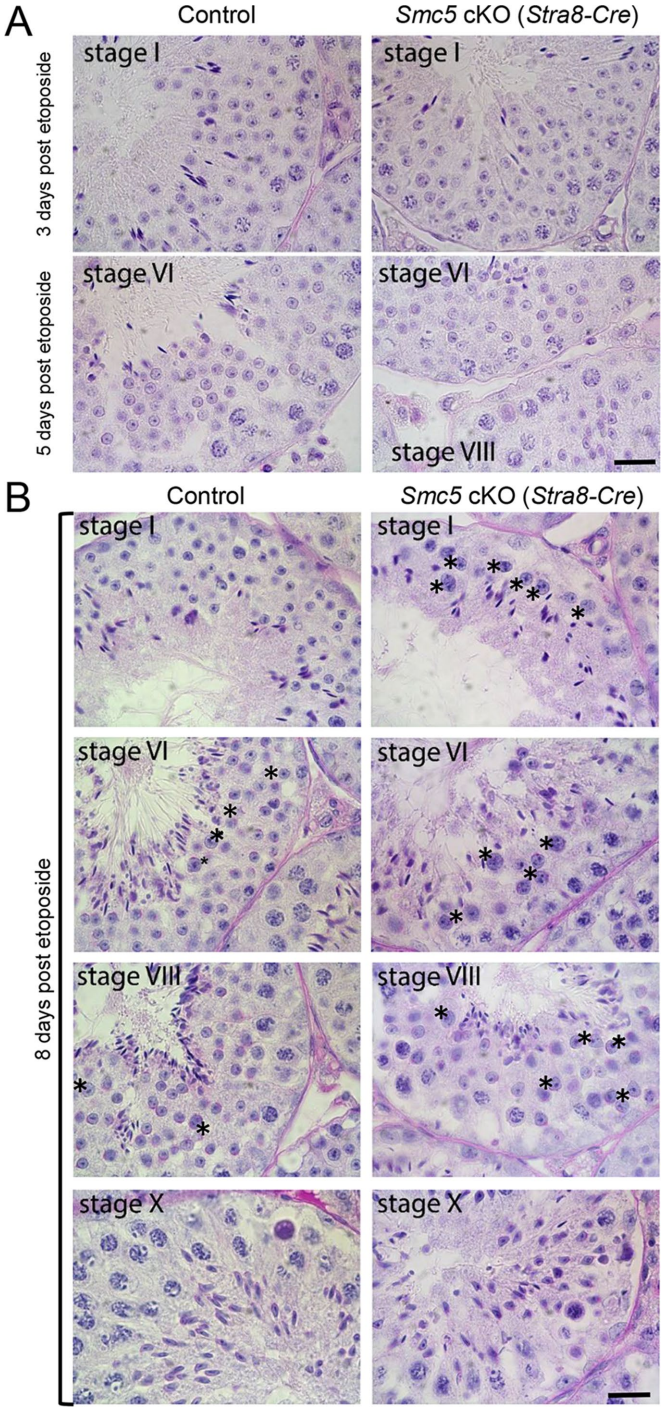

FIGURE 8: Conditional mutation of *Smc5* results in increased sensitivity to etoposide, producing a similar phenotype seen for irradiation. (A, B) Periodic acid–Schiff stained tubule cross-sections of adult control and *Smc5* cKO (*Stra8-Cre*) testes extracted at 3, 5, or 8 d postexposure to etoposide. *Smc5* cKO testes have increased numbers of abnormal enlarged round spermatids (*) at 8 d postexposure. Roman numerals correspond to the seminiferous tubule stage. Mice were ≥8 wk old. Scale bar: 20 μm.

immunostaining procedures. Primary antibodies and dilution used are presented in Supplemental Table S2. Secondary antibodies against human, rabbit, rat, mouse, and guinea pig immunoglobulin G (IgG) and conjugated to Alexa 350, 488, 568, or 633 (Life Technologies) were used at 1:500 dilution.

Mouse germ cell isolation and culture

Isolation of mixed germ cells from testes was performed using techniques previously described (Bellve, 1993; La Salle *et al.*, 2009). Leptotene/zygotene and pachytene-stage spermatocytes and round spermatids were enriched using a 2–4% bovine serum albumin gradient generated in a STA-PUT sedimentation chamber (ProScience), as previously described (La Salle *et al.*, 2009).

Protein analyses

For protein level analyses, proteins were extracted from germ cells using RIPA buffer (Santa Cruz) containing 1× protease inhibitor cocktail (Roche). Protein concentration was calculated using a BCA protein assay kit (Pierce). Lanes of 4–15% gradient SDS polyacrylamide gels (Bio-Rad) were loaded with 20 μl of 1 mg/ml protein extract. For STA-PUT, 20 μl of 0.1 mg/ml protein extracts from purified leptotene/zygotene and pachytene/diplotene stage spermatocytes and round spermatids were loaded per lane on SDS polyacrylamide gels. Following protein separation via standard SDS–PAGE, proteins were transferred to polyvinylidene difluoride (PVDF) membranes using the Trans-Blot Turbo Western transfer system (Bio-Rad). Primary antibodies and dilution used are presented in Supplemental Table S2. At a 1:5000 dilution, goat anti-mouse (62-6520) and goat anti-rabbit (A10533) horseradish peroxidase–conjugated antibodies (Invitrogen) were used as secondary antibodies. The presence of antibodies on the PVDF membranes was detected via treatment with Pierce ECL Western blotting substrate (Thermo Scientific) and captured using the Syngene XR5 gel documentation system. Protein levels were assessed using Image J (NIH).

Chromatin spread analyses

Germ cell chromatin spreads were prepared as previously described (Jordan *et al.*, 2012), or with some modifications. Briefly, germ cells were placed in 50% hypotonic buffer (30 mM Tris, 50 mM sucrose, 17 mM trisodium citrate dihydrate, 5 mM EDTA, 2.5 mM dithiothreitol) for 8 min. The cells were then resuspended in a second hypotonic buffer (1:1 of PBS and 100 μM sucrose). The cell suspension was fixed using 1% PFA on a glass slide for 1 h in a humid chamber. The slides were air dried for 1 h, washed in 0.4% Photo-Flo (Kodak) in H_2O overnight, and dried again for 30 min. The slides were immunolabeled immediately afterward. Primary antibodies and dilution used are presented in Supplemental Table S2. Rat–anti-SMC5 (AP6962B) and rat–anti-NSE4a (AP6962A) antibodies were prepared using peptide sequences, cys-PHMLEPNRWNLKAF and ys-PKPRSDRPRQPRMIE, respectively (Neobiolabs). Secondary antibodies against human, rabbit, rat, mouse, and guinea pig IgG and conjugated to Alexa 350, 488, 568, or 633 (Life Technologies) were used at a dilution of 1:500.

Spermatocyte squash preparation

Spermatocyte squashes were performed as previously described (Wellard *et al.*, 2018). Briefly, minced seminiferous tubules from 23-d-old male mice were fixed in freshly prepared 2% formaldehyde in 1× PBS containing 0.1% Triton X-100. After 5 min, several seminiferous tubule fragments were placed on a slide and squashed, and the coverslip removed after freezing in liquid nitrogen. Slides were washed with 1× PBS and immunostained immediately afterward.

Microscopy

Images from chromatin spread, tubule squash, and testis cryosection preparations were captured using a Zeiss CellObserver Z1 microscope linked to an ORCA-Flash 4.0 CMOS camera (Hamamatsu). Testis sections stained with hematoxylin and eosin or PAS staining

were captured using a Zeiss AxioImager A2 microscope linked to an AxioCam ERc5s camera. Images were analyzed with Zeiss ZEN 2012 blue edition image software including foci and length measurement capabilities. Photoshop (Adobe) was used to prepare figure images.

ACKNOWLEDGMENTS

We thank Sakshi Khurana and Stephen Wellard for technical support. We are grateful to Paula Cohen and Mitch Eddy for mice harboring the *Spo11-Cre* and *Hspa2-Cre* transgenes, respectively. This work was supported by a UK-US Fulbright Distinguished Scholar Award to P.W.J., National Institutes of Health (NIH) K99/R00 HD-069458 to P.W.J, NIH R01 HD-33816 to M.A.H., NIH R01 GM-117155 to P.W.J., institutional NIH Cancer Center award CA34196 to The Jackson Laboratory, and training grant CA009110 fellowship to G.H.

REFERENCES

Ampatzidou E, Irmisch A, O'Connell MJ, Murray JM (2006). Smc5/6 is required for repair at collapsed replication forks. Mol Cell Biol 26, 9387–9401.

Andrews EA, Palecek J, Sergeant J, Taylor E, Lehmann AR, Watts FZ (2005). Nse2, a component of the Smc5-6 complex, is a SUMO ligase required for the response to DNA damage. Mol Cell Biol 25, 185–196.

Bannister LA, Reinholdt LG, Munroe RJ, Schimenti JC (2004). Positional cloning and characterization of mouse *mei8*, a disrupted allelle of the meiotic cohesin *Rec8*. Genesis 40, 184–194.

Baudrimont A, Penkner A, Woglar A, Mamnun YM, Hulek M, Struck C, Schnabel R, Loidl J, Jantsch V (2011). A new thermosensitive smc-3 allele reveals involvement of cohesin in homologous recombination in *C. elegans*. PLoS One 6, e24799.

Bellve AR (1993). Purification, culture, and fractionation of spermatogenic cells. Methods Enzymol 225, 84–113.

Bermúdez-López M, Ceschia A, de Piccoli G, Colomina N, Pasero P, Aragón L, Torres-Rosell J (2010). The Smc5/6 complex is required for dissolution of DNA-mediated sister chromatid linkages. Nucleic Acids Res 38, 6502–6512.

Bickel JS, Chen L, Hayward J, Yeap SL, Alkers AE, Chan RC (2010). Structural maintenance of chromosomes (SMC) proteins promote homolog-independent recombination repair in meiosis crucial for germ cell genomic stability. PLos Genet 6, e1001028.

Biswas U, Hempel K, Llano E, Pendas A, Jessberger R (2016). Distinct roles of meiosis-specific cohesin complexes in mammalian spermatogenesis. PLos Genet 12, e1006389.

Branzei D, Sollier J, Liberi G, Zhao X, Maeda D, Seki M, Enomoto T, Ohta K, Foiani M (2006). Ubc9- and mms21-mediated sumoylation counteracts recombinogenic events at damaged replication forks. Cell 127, 509–522.

Brito IL, Yu H-G, Amon A (2010). Condensins promote coorientation of sister chromatids during meiosis I in budding yeast. Genetics 185, 55–64.

Caburet S, Arboleda VA, Llano E, Overbeek PA, Barbero JL, Oka K, Harrison W, Vaiman D, Ben-Neriah Z, García-Tuñón I, *et al*. (2014). Mutant cohesin in premature ovarian failure. N Engl J Med 370, 943–949.

Copsey A, Tang S, Jordan PW, Blitzblau HG, Newcombe S, Chan AC, Newnham L, Li Z, Gray S, Herbert AD, *et al*. (2013). Smc5/6 coordinates formation and resolution of joint molecules with chromosome morphology to ensure meiotic divisions. PLos Genet 9, e1004071.

Dexheimer TS (2013). DNA repair pathways and mechanisms. In: DNA Repair of Cancer Stem Cells, ed. LA Mathews, SM Cabarcas, and EM Hurt, Dordrecht: Springer Netherlands, 19–32.

Doyle JM, Gao J, Wang J, Yang M, Potts PR (2010). MAGE-RING protein complexes comprise a family of E3 ubiquitin ligases. Mol Cell 39, 963–974.

Forand A, Dutrillaux B, Bernardino-Sgherri J (2004). γ-H2AX expression pattern in non-irradiated neonatal mouse germ cells and after low-dose γ-radiation: relationships between chromatid breaks and DNA double-strand breaks. Biol Reprod 71, 643–649.

Gallardo T, Shirley L, John GB, Castrillon DH (2007). Generation of a germ cell-specific mouse transgenic Cre line, Vasa-Cre. Genesis 45, 413–417.

Gallego-Paez LM, Tanaka H, Bando M, Takahashi M, Nozaki N, Nakato R, Shirahige K, Hirota T (2014). Smc5/6-mediated regulation of replication progression contributes to chromosome assembly during mitosis in human cells. Mol Biol Cell 25, 302–317.

Gómez R, Jordan PW, Viera A, Alsheimer M, Fukuda T, Jessberger R, Llano E, Pendás AM, Handel MA, Suja JA (2013). Dynamic localization of SMC5/6 complex proteins during mammalian meiosis and mitosis suggests functions in distinct chromosome processes. J Cell Sci 126, 4239–4252.

Hamer G, Roepers-Gajadien HL, van Duyn-Goedhart A, Gademan IS, Kal HB, van Buul PPW, de Rooij DG (2003). DNA double-strand breaks and γ-H2AX signaling in the testis. Biol Reprod 68, 628–634.

Heisig P (2009). Type II topoisomerases—inhibitors, repair mechanisms and mutations. Mutagenesis 24, 465–469.

Herrán Y, Gutiérrez-Caballero C, Sánchez-Martín M, Hernández T, Viera A, Barbero JL, de Álava E, de Rooij DG, Suja JÁ, Llano E, Pendás AM (2011). The cohesin subunit RAD21L functions in meiotic synapsis and exhibits sexual dimorphism in fertility. EMBO J 30, 3091–3105.

Hodges CA, Revenkova E, Jessberger R, Hassold TJ, Hunt PA (2005). SMC1β-deficient female mice provide evidence that cohesins are a missing link in age-related nondisjunction. Nat Genet 37, 1351–1355.

Holloway JK, Booth J, Edelmann W, McGowan CH, Cohen PE (2008). MUS81 generates a subset of MLH1-MLH3–independent crossovers in mammalian meiosis. PLos Genet 4, e1000186.

Holloway JK, Mohan S, Balmus G, Sun X, Modzelewski A, Borst PL, Freire R, Weiss RS, Cohen PE (2011). Mammalian BTBD12 (SLX4) protects against genomic instability during mammalian spermatogenesis. PLos Genet 7, e1002094.

Hong Y, Sonneville R, Agostinho A, Meier B, Wang B, Blow JJ, Gartner A (2016). The SMC-5/6 complex and the HIM-6 (BLM) helicase synergistically promote meiotic recombination intermediate processing and chromosome maturation during *Caenorhabditis elegans* meiosis. PLos Genet 12, e1005872.

Hopkins J, Hwang G, Jacob J, Sapp N, Bedigian R, Oka K, Overbeek P, Murray S, Jordan PW (2014). Meiosis-specific cohesin component, Stag3 is essential for maintaining centromere chromatid cohesion, and required for DNA repair and synapsis between homologous chromosomes. PLos Genet 10, e1004413.

Houlard M, Godwin J, Metson J, Lee J, Hirano T, Nasmyth K (2015). Condensin confers the longitudinal rigidity of chromosomes. Nat Cell Biol 17, 771–781.

Hudson JJ, Bednarova K, Kozakova L, Liao C, Guerineau M, Colnaghi R, Vidot S, Marek J, Bathula SR, Lehmann AR, Palecek J (2011). Interactions between the Nse3 and Nse4 components of the SMC5-6 complex identify evolutionarily conserved interactions between MAGE and EID families. PLoS One 6, e17270.

Hwang G, Sun F, O'Brien M, Eppig JJ, Handel MA, Jordan PW (2017). SMC5/6 is required for the formation of segregation-competent bivalent chromosomes during meiosis I in mouse oocytes. Development 144, 1648–1660.

Inselman AL, Nakamura N, Brown PR, Willis WD, Goulding EH, Eddy EM (2010). Heat shock protein 2 promoter drives Cre expression in spermatocytes of transgenic mice. Genesis 48, 114–120.

Jordan PW, Karppinen J, Handel MA (2012). Polo-like kinase is required for synaptonemal complex disassembly and phosphorylation in mouse spermatocytes. J Cell Sci 125, 5061–5072.

Kauppi L, Barchi M, Baudat F, Romanienko PJ, Keeney S, Jasin M (2011). Distinct properties of the XY pseudoautosomal region crucial for male meiosis. Science 331, 916–920.

Kent TGMD (2014). Checking the pulse of vitamin A metabolism and signaling during mammalian spermatogenesis. J Dev Biol 2, 34–39.

Klein F, Mahr P, Galova M, Buonomo SB, Michaelis C, Nairz K, Nasmyth K (1999). A central role for cohesins in sister chromatid cohesion, formation of axial elements, and recombination during yeast meiosis. Cell 98, 91–103.

Kozakova L, Vondrova L, Stejskal K, Charalabous P, Kolesar P, Lehmann AR, Uldrijan S, Sanderson CM, Zdrahal Z, Palecek JJ (2015). The melanoma-associated antigen 1 (MAGEA1) protein stimulates the E3 ubiquitin-ligase activity of TRIM31 within a TRIM31-MAGEA1-NSE4 complex. Cell Cycle 14, 920–930.

Lao JP, Hunter N (2010). Trying to avoid your sister. PLoS Biol 8, e1000519.

La Salle S, Sun F, Handel MA (2009). Isolation and short-term culture of mouse spermatocytes for analysis of meiosis. Methods Mol Biol 558, 279–297.

Lee J, Ogushi S, Saitou M, Hirano T (2011). Condensins I and II are essential for construction of bivalent chromosomes in mouse oocytes. Mol Biol Cell 22, 3465–3477.

Lee JS, Takahashi T, Hagiwara A, Yoneyama C, Itoh M, Sasabe T, Muranishi S, Tashima S (1995). Safety and efficacy of intraperitoneal injection of etoposide in oil suspension in mice with peritoneal carcinomatosis. Cancer Chemother Pharmacol 36, 211–216.

Lilienthal I, Kanno T, Sjögren C (2013). Inhibition of the Smc5/6 complex during meiosis perturbs joint molecule formation and resolution without significantly changing crossover or non-crossover levels. PLos Genet 9, e1003898.

Llano E, Gomez-H L, García-Tuñón I, Sánchez-Martín M, Caburet S, Barbero JL, Schimenti JC, Veitia RA, Pendas AM (2014). STAG3 is a strong candidate gene for male infertility. Hum Mol Genet 23, 3421–3431.

Lyndaker AM, Lim PX, Mleczko JM, Diggins CE, Holloway JK, Holmes RJ, Kan R, Schlafer DH, Freire R, Cohen PE, Weiss RS (2013). Conditional inactivation of the DNA damage response gene Hus1 in mouse testis reveals separable roles for components of the RAD9-RAD1-HUS1 complex in meiotic chromosome maintenance. PLos Genet 9, e1003320.

Marchetti F, Pearson FS, Bishop JB, Wyrobek AJ (2006). Etoposide induces chromosomal abnormalities in mouse spermatocytes and stem cell spermatogonia. Hum Reprod 21, 888–895.

Mets DG, Meyer BJ (2009). Condensins regulate meiotic DNA break distribution, thus crossover frequency, by controlling chromosome structure. Cell 139, 73–86.

Moens PB, Chen DJ, Shen Z, Kolas N, Tarsounas M, Heng HH, Spyropoulos B (1997). Rad51 immunocytology in rat and mouse spermatocytes and oocytes. Chromosoma 106, 207–215.

Murray JM, Carr AM (2008). Smc5/6: a link between DNA repair and unidirectional replication? Nat Rev Mol Cell Biol 9, 177–182.

Palecek J, Vidot S, Feng M, Doherty AJ, Lehmann AR (2006). The Smc5-Smc6 DNA repair complex. Bridging of the Smc5-Smc6 heads by the KLEISIN, Nse4, and non-Kleisin subunits. J Biol Chem 281, 36952–36959.

Pasierbek P, Födermayr M, Jantsch V, Jantsch M, Schweizer D, Loidl J (2003). The *Caenorhabditis elegans* SCC-3 homologue is required for meiotic synapsis and for proper chromosome disjunction in mitosis and meiosis. Exp Cell Res 289, 245–255.

Payne F, Colnaghi R, Rocha N, Seth A, Harris J, Carpenter G, Bottomley WE, Wheeler E, Wong S, Saudek V, *et al*. (2014). Hypomorphism in human NSMCE2 linked to primordial dwarfism and insulin resistance. J Clin Invest 124, 4028–4038.

Phadnis N, Cipak L, Polakova S, Hyppa RW, Cipakova I, Anrather D, Karvaiova L, Mechtler K, Smith GR, Gregan J (2015). Casein kinase 1 and phosphorylation of cohesin subunit Rec11 (SA3) promote meiotic recombination through linear element formation. PLos Genet 11, e1005225.

Potts PR, Yu H (2007). The SMC5/6 complex maintains telomere length in ALT cancer cells through SUMOylation of telomere-binding proteins. Nat Struct Mol Biol 14, 581–590.

Revenkova E, Eijpe M, Heyting C, Hodges CA, Hunt PA, Liebe B, Scherthan H, Jessberger R (2004). Cohesin SMC1 β is required for meiotic chromosome dynamics, sister chromatid cohesion and DNA recombination. Nat Cell Biol 6, 555–562.

Sadate-Ngatchou PI, Payne CJ, Dearth AT, Braun RE (2008). Cre recombinase activity specific to postnatal, premeiotic male germ cells in transgenic mice. Genesis 46, 738–742.

Sakuno T, Watanabe Y (2015). Phosphorylation of cohesin Rec11/SA3 by casein kinase 1 promotes homologous recombination by assembling the meiotic chromosome axis. Dev Cell 32, 220–230.

Severson AF, Meyer BJ (2014). Divergent kleisin subunits of cohesin specify mechanisms to tether and release meiotic chromosomes. Elife 3, e03467.

Ventelä S, Côme C, Mäkelä J-A, Hobbs RM, Mannermaa L, Kallajoki M, Chan EK, Pandolfi PP, Toppari J, Westermarck J (2012). CIP2A promotes proliferation of spermatogonial progenitor cells and spermatogenesis in mice. PLoS One 7, e33209.

Verver DE, Hwang GH, Jordan PW, Hamer G (2016a). Resolving complex chromosome structures during meiosis: versatile deployment of Smc5/6. Chromosoma 125, 15–27.

Verver DE, van Pelt AMM, Repping S, Hamer G (2013). Role for rodent Smc6 in pericentromeric heterochromatin domains during spermatogonial differentiation and meiosis. Cell Death Dis 4, e749.

Verver DE, Zheng Y, Speijer D, Hoebe R, Dekker HL, Repping S, Stap J, Hamer G (2016b). Non-SMC element 2 (NSMCE2) of the SMC5/6 complex helps to resolve topological stress. Int J Mol Sci 17, 1782.

Ward A, Hopkins J, Mckay M, Murray S, Jordan PW (2016). Genetic interactions between the meiosis-specific cohesin components, STAG3, REC8, and RAD21L. G3 (Bethesda) 6, 1713–1724.

Watanabe Y, Nurse P (1999). Cohesin Rec8 is required for reductional chromosome segregation at meiosis. Nature 400, 461–464.

Wehrkamp-Richter S, Hyppa RW, Prudden J, Smith GR, Boddy MN (2012). Meiotic DNA joint molecule resolution depends on Nse5-Nse6 of the Smc5-Smc6 holocomplex. Nucleic Acids Res 40, 9633–9646.

Wellard SR, Hopkins J, Jordan PW (2018). A seminiferous tubule squash technique for the cytological analysis of spermatogenesis using the mouse model. J Vis Exp 132, e56453.

Winters T, McNicoll F, Jessberger R (2014). Meiotic cohesin STAG3 is required for chromosome axis formation and sister chromatid cohesion. EMBO J 33, 1256–1270.

Wojtasz L, Daniel K, Roig I, Bolcun-Filas E, Xu H, Boonsanay V, Eckmann CR, Cooke HJ, Jasin M, Keeney S, *et al*. (2009). Mouse HORMAD1 and HORMAD2, two conserved meiotic chromosomal proteins, are depleted from synapsed chromosome axes with the help of TRIP13 AAA-ATPase. PLos Genet 5, e1000702.

Wu N, Kong X, Ji Z, Zeng W, Potts PR, Yokomori K, Yu H (2012). Scc1 sumoylation by Mms21 promotes sister chromatid recombination through counteracting Wapl. Genes Dev 26, 1473–1485.

Xaver M, Huang L, Chen D, Klein F (2013). Smc5/6-Mms21 prevents and eliminates inappropriate recombination intermediates in meiosis. PLos Genet 9, e1004067.

Xu H, Beasley MD, Warren WD, van der Horst GTJ, McKay MJ (2005). Absence of mouse REC8 cohesin promotes synapsis of sister chromatids in meiosis. Dev Cell 8, 949–961.

Zhao X, Blobel G (2005). A SUMO ligase is part of a nuclear multiprotein complex that affects DNA repair and chromosomal organization. Proc Natl Acad Sci USA 102, 4777–4782.

Zheng Y, Jongejan A, Mulder CL, Mastenbroek S, Repping S, Wang Y, Li J, Hamer G (2017). Trivial role for NSMCE2 during in vitro proliferation and differentiation of male germline stem cells. Reproduction 154, 81–95.